- The viscoelastic PPT model, a modified Waters' B′ model ensures controlled transport of nanoparticles used to deliver drug into targeted cells of tumor sites.
- The flow behavior of non-Newtonian biological fluid i.e. bloods useful in artificial organ systems, dialysis machines, etc.
- The controlled flow of nanoparticles aids in design of microfluidic devices and releasing drugs.

2. Formation of the model

The proposed flow phenomena based on the consideration of the viscoelastic nanofluid peristaltic flow comprised of Phan-Thien-Tanner model nanoliquid, Here, the flow passes via asymmetric vertical channels where the thickness of the channel is homogenous and described as $d_1 + d_2$. In the case of the proposed model, the peristaltic flow is carried by low amplitudes a_1 and b_1 at a constant speed c,and, sinusoidal peristaltic wave of wavelength λ. Flow properties are mention for the coordinate system $(\overline{X}, \overline{Y})$, in which the $\overline{X}$-axis is placed toward the center of the channel while the $\overline{Y}$-axis is perpendicular to it. The graphical behaviour is projected in Fig. 1 The schematic presentation of the model. However, the impact of magnetization is carried out for the inclusion of transverse magnetic field. A uniform transverse magnetism of strength B_0 is employed toward the normal to the flow. The structure of all these components is illustrated for the irregular temperatures at upper and lower walls, and concentrations (T_0, C_0) and (T_1, C_1), respectively.

$$\overline{Y} = \overline{H}_1 = d_1 + a_1 \cos\left(\frac{2\pi}{\lambda}(\overline{x} - c\overline{t})\right) \tag{1}$$

$$\overline{Y} = \overline{H}_2 = -d_2 - b_1 \cos\left(\frac{2\pi}{\lambda}(\overline{x} - c\overline{t})\right) \tag{2}$$

The transformations used listed below with constraints $(\overline{x}, \overline{y})$ are modified into stationary constraints $(\overline{X}, \overline{Y})$:

$$\overline{x} = \overline{X} - c\overline{t}, \overline{y} = \overline{Y}, \overline{p} = \overline{P}(x,t), \overline{u} = \overline{U} - c, \overline{\chi} = \overline{\psi} - \frac{R^2}{2} \tag{3}$$

In particular, $\overline{P}$ and $\overline{p}$ indicate pressures, whereas the stream functions $\overline{\chi}$ and $\overline{\psi}$ and, $\overline{U}$ and $\overline{u}$ stand for velocities along moving vis-a-vis stationary coordinates.

The proposed gold nanoparticles for the mixed convection problem, the density is assumed as;

$$\left.\begin{array}{l} \rho = (1-\overline{\phi})\rho_f + \overline{\phi}\rho_p, \\ \rho \cong (1-\overline{\phi})\{\rho_{f_0}(1-\beta(T-T_1))\} + \overline{\phi}\rho_p \end{array}\right\} \tag{4}$$

Here, ρ_p represents the base fluid's density, β denotes the volumetric expansion coefficient, ρ_{f_0} corresponds to the nanofluid's density at the reference temperature, ρ_f indicates the density of the gold nanoparticles, $\overline{T}_1$ refers to the reference temperature, $\overline{T}$ signifies the fluid temperature, and $\overline{\phi}$ denotes the volume fraction of the solid nanoparticles.

The proposed governing equations are.

$$\frac{d\overline{u}}{d\overline{x}} + \frac{d\overline{v}}{d\overline{y}} = 0, \tag{5}$$

$$\rho_f\left(\frac{d\overline{u}}{d\overline{t}} + \overline{u}\frac{d\overline{u}}{d\overline{x}} + \overline{v}\frac{d\overline{u}}{d\overline{y}}\right) = -\frac{d\overline{p}}{d\overline{x}} + \frac{d}{d\overline{y}}\overline{\tau}_{\overline{xy}} + \frac{d}{d\overline{x}}\overline{\tau}_{\overline{xx}} + \frac{\sigma B_0^2}{1-\Omega^2}(\overline{u} + \Omega\overline{v}) + \overline{\phi}\rho_p + (1-\overline{\phi})\left\{\rho_{f_0}\left(1 - \beta(T-T_0)g - g(\rho_p - \rho_{f_0})(F-F_0)\right\}\right. \tag{6}$$

$$\rho_f\left(\frac{d\overline{v}}{d\overline{t}} + \overline{u}\frac{d\overline{v}}{d\overline{x}} + \overline{v}\frac{d\overline{v}}{d\overline{y}}\right) = -\frac{d\overline{p}}{d\overline{y}} + \frac{d}{d\overline{x}}\overline{\tau}_{\overline{xy}} + \frac{d}{d\overline{y}}\overline{\tau}_{\overline{yy}} + \frac{\sigma B_0^2}{1-\Omega^2}(\Omega\overline{u} - \overline{v}), \tag{7}$$

$$(\rho c_p)_f\left(\frac{dT}{dt} + \overline{u}\frac{dT}{d\overline{x}} + \overline{v}\frac{dT}{d\overline{y}}\right) = k\left(\frac{d^2T}{d\overline{x}^2} + \frac{d^2T}{d\overline{y}^2}\right) + (\rho c)_p D_B\left(\frac{dF}{d\overline{x}}\frac{dT}{d\overline{x}} + \frac{dF}{d\overline{y}}\frac{dT}{d\overline{y}}\right) + (\rho c)_p\frac{D_T}{T_0}\left\{\left(\frac{dT}{d\overline{x}}\right)^2 + \left(\frac{dT}{d\overline{y}}\right)^2\right\} + D_{TC}\left(\frac{d^2C}{d\overline{x}^2} + \frac{d^2C}{d\overline{y}^2}\right) - \frac{\partial w_r}{\partial \overline{y}} + S \tag{8}$$

$$\left(\frac{dC}{d\overline{t}} + \overline{u}\frac{dC}{d\overline{x}} + \overline{v}\frac{dC}{d\overline{y}}\right) = D_{CT}\left(\frac{d^2T}{d\overline{x}^2} + \frac{d^2T}{d\overline{y}^2}\right) + D_S\left(\frac{d^2T}{d\overline{x}^2} + \frac{d^2C}{d\overline{y}^2}\right) \tag{9}$$

$$\left(\frac{dF}{d\overline{t}} + \overline{u}\frac{dF}{d\overline{x}} + \overline{v}\frac{dF}{d\overline{y}}\right) = D_B\left(\frac{d^2F}{d\overline{x}^2} + \frac{d^2F}{d\overline{y}^2}\right) + \frac{D_T}{T_0}\left(\frac{d^2T}{d\overline{x}^2} + \frac{d^2T}{d\overline{y}^2}\right) \tag{10}$$

However, the surface conditions fit for the proposed problem are;

$$\frac{d\overline{u}}{d\overline{y}}=\frac{q}{2},\overline{u}-\alpha\overline{\tau}_{\overline{xy}}=-1,T=T_0,C=C_0,F=F_0\ \ at\ \ \overline{Y}=\overline{H}_1=d_1+a_1\cos\left(\frac{2\pi}{\lambda}(\overline{x}-c\overline{t})\right) \tag{11a}$$

$$\frac{d\overline{u}}{d\overline{y}}=\frac{q}{2},\overline{u}-\alpha\overline{\tau}_{\overline{xy}}=-1,T=T_1,C=C_1,F=F_1\ \ at\ \ \overline{Y}=\overline{H}_2=-d_2-b_1\cos\left(\frac{2\pi}{\lambda}(\overline{x}-c\overline{t})+\varphi\right) \tag{11b}$$

The rheological behaviour of the non-Newtonian fluid is character by the assumption of PTT model. As a refinement, the model is developed from the Oldroyd-B model, it effectively represents the flow properties of fluids exhibiting the characteristic of both shear-thinning and viscoelastic properties, including polymer melts, suspensions, and other intricate fluid systems. It accounts for fluid viscoelasticity while incorporating shear rate-dependent effects.

The governing equation for the Phan-Thien-Tanner fluid is

$$\overline{\tau}_{\overline{xy}}+2We^2\overline{\tau}_{\overline{xy}}{}^3=\frac{d\overline{u}}{d\overline{y}} \tag{12}$$

In energy distribution, heat energy is 1-D and the heat flux above $\overline{Y}$ direction w_r is assumed by using Rosseland's approximation, then the radiative heat flux is of the form;

$$w_r=-16\frac{\sigma' T_1{}^3}{3k'}\frac{\partial T}{\partial\overline{y}} \tag{13}$$

where k' and σ' denote the mean absorption and the Stefan-Boltzmann constant.

The dimensionless quantities are.

$$\left.\begin{aligned}
&x=\frac{\overline{x}}{\lambda},y=\frac{\overline{y}}{d_1},u=\frac{\overline{u}}{c},t=\frac{c\overline{t}}{\lambda},p=\frac{\overline{p}a^2}{\lambda\mu c},a=\frac{a_1}{d_1},b=\frac{b_1}{d_1},\delta=\frac{d_1}{\lambda},\Pr=\frac{\mu c_p}{k},Ec=\frac{c^2}{c_p(T_1-T_0)},h_1=\frac{H_1}{d_1},\\
&h_2=\frac{H_2}{d_1},d=\frac{d_2}{d_1},Rd=\frac{16\sigma T_1^3}{3kk'},\theta=\frac{T-T_0}{T_1-T_0},\phi=\frac{C-C_0}{C_1-C_0},\gamma=\frac{F-F_0}{F_1-F_0},Mn=\sqrt{\frac{\sigma}{\mu}}B_0a,N=Ec\times\Pr\\
&Nb=D_B\frac{(\rho c)_p(C_1-C_0)}{k},Nt=\frac{(\rho c)_p(T_1-T_0)}{T_0k},Nc_t=\frac{D_{CT}(T_1-T_0)}{D_S(\phi_1-\phi_0)},Nt_c=\frac{(\rho c_1)_fD_{TC}(\phi_1-\phi_0)}{D_S(T_1-T_0)},\beta=\frac{S\lambda^2}{k(T_1-T_0)}\\
&Gr_c=\frac{\rho_p(C_1-C_0)d_1{}^2}{c\mu},Gr_t=\frac{\rho_{f_0}(1-C)(1-\beta)gd_1{}^2(T_1-T_0)}{c\mu},Gr_f=\frac{(\rho c_1)_fD_{TC}(C_1-C_0)}{k(\overline{T}_1-\overline{T}_0)},We=\frac{kc}{a}
\end{aligned}\right\}$$

Using the aforementioned non-dimensional factors, the governing Eqs. (5)–(10) along with (12) and (13), as well as BC's (11a) and (11b), are

$$\frac{d^4\psi}{dy^4}-\frac{Mn^2}{1+\Omega^2}\frac{d^2\psi}{dy^2}+Gr_t\theta+Gr_c\phi-Gr_f\gamma-2We^2\left(\frac{Mn^2}{1+\Omega^2}\frac{d^2\psi}{dy^2}-Gr_t\theta-Gr_c\phi+Gr_f\gamma\right)^3=0 \tag{14}$$

$$(1+Rd\,\Pr)\frac{d^2\theta}{dy^2}+Nb\,\Pr\frac{d\theta}{dy}\frac{d\gamma}{dy}+Nt\,\Pr\left(\frac{d\theta}{dy}\right)^2+Nt_c\,\Pr\frac{d^2\phi}{dy^2}+\beta=0 \tag{15}$$

$$\frac{d^2\phi}{dy^2}+Nc_t\frac{d^2\theta}{dy^2}=0 \tag{16}$$

$$\frac{d^2\gamma}{dy^2}+\frac{Nt}{Nb}\frac{d^2\theta}{dy^2}=0 \tag{17}$$

Consistently, the constructed surface assumptions are

$$\psi=\frac{f}{2},\frac{d\psi}{dy}-\alpha\frac{d^2\psi}{dy^2}=-1,\theta=0,\phi=0,\gamma=0\quad at\ y=h_1=1+a\cos\left\{\frac{2\pi}{\lambda}(x-t)\right\} \tag{18a}$$

$$\psi=-\frac{f}{2},\frac{d\psi}{dy}+\alpha\frac{d^2\psi}{dy^2}=-1,\theta=1,\phi=1,\gamma=1\ \ at\ y=h_2=-d-b\cos\left\{\frac{2\pi}{\lambda}(x-t)+\varphi\right\} \tag{18b}$$

The mean flow (Θ) relating to steady ordinates and f, connected moving references presented by $\Theta=f+1$ where

$$f=\int_{h_1}^{h_2}\frac{d\psi}{dy}dy \tag{19}$$

In which $\Theta=\frac{Q}{cd_1}$ *and* $f=\frac{q}{cd_1}$

3. Numerical solution

The differential equations 14–17 along with boundary conditions (18a-18b) that control the problem are extremely complicated and highly nonlinear. Therefore, a numerical approach, the Runge-Kutta 4th order with Shooting technique is proposed for solving ordinary differential equations. Further, it integrates the methodologies of Runge-Kutta 4th order and Shooting analysis. In this numerical strategy, estimating the initial guess is one of the most important jobs. For required persistence, Eqs. 14–17 are dispended in first order with the following variables:

$$\left.\begin{aligned} L_1 = \psi, L_2 = \psi', L_3 = \psi'', L_4 = \psi''', L_4' = \psi'''', \\ L_5 = \theta, L_6 = \theta', L_6' = \theta'', \\ L_7 = \phi, L_8 = \phi', L_8' = \phi'', \\ L_9 = \gamma, L_{10} = \gamma', L_{10}' = \gamma''. \end{aligned}\right\} \tag{20}$$

After using the above variables Eqs. 14–17 are converted into the following set of first order differential equations

$$\left.\begin{aligned} L_4' = 2We^2\left[\frac{M_n^2}{1+\Omega^2}L_3 - Gr_t\, L_5 - Gr_c\, L_7 + Gr_f\, L_9\right]^3 + \\ \frac{M_n^2}{1+\Omega^2}L_3 - Gr_t\, L_5 - Gr_c\, L_7 + Gr_f\, L_9 \end{aligned}\right\} \tag{21}$$

$$L_6' = -\frac{1}{\left(1 + Rd\, Pr - Nt_c\, Pr\, \frac{Nt}{Nb}\right)}\left[Nb\, Pr\, L_6\, L_{10} + Nt\, Pr\, L_6^2 + \beta\right] \tag{22}$$

$$L_8' = \frac{Nt_c}{\left(1 + Rd\, Pr - Nt_c\, Pr\, \frac{Nt}{Nb}\right)}\left[Nb\, Pr\, L_6\, L_{10} + Nt\, Pr\, L_6^2 + \beta\right] \tag{23}$$

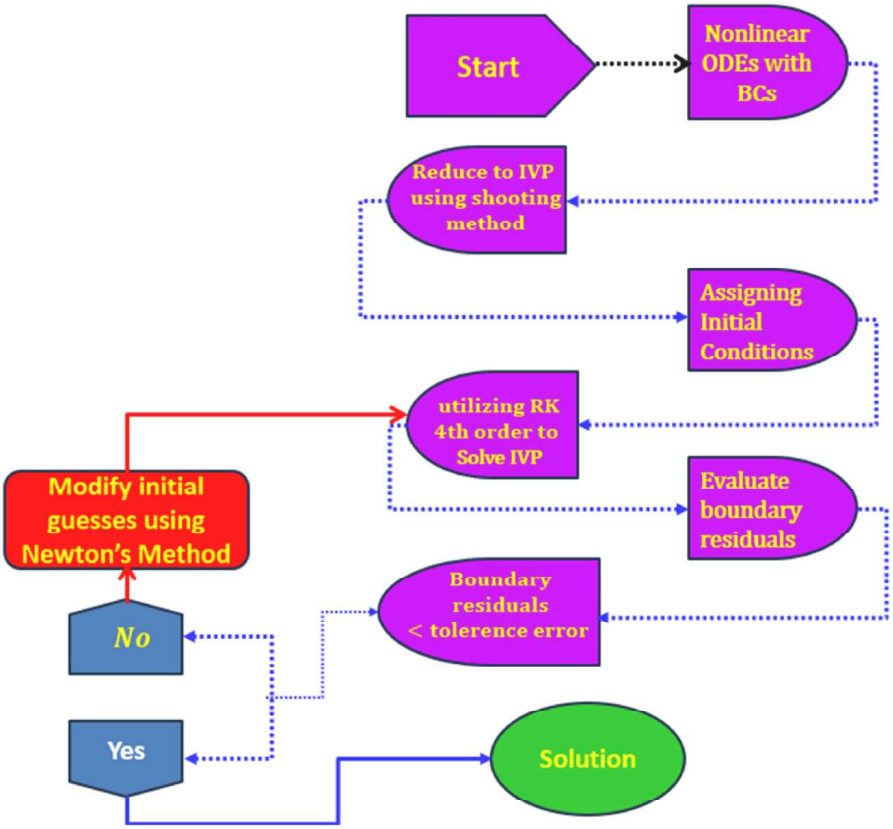

Fig. 2. Flow chart of solution methodology.

$$L'_{10} = \frac{Nt}{Nb}\frac{1}{\left(1 + Rd\,Pr - Nt_c\,Pr\,\frac{Nt}{Nb}\right)}\left[Nb\,Pr\,L_6\,L_{10} + Nt\,Pr\,L_6^2 + \beta\right] \tag{24}$$

subjected to boundary conditions using (20)

$$\left.\begin{aligned} L_1 = \frac{f}{2}, L_2 - \alpha L_3 = -1, L_5 = 0, L_7 = 0, L_9 = 0 \\ at\ y = h_1 = 1 + a\,Cos\left(\frac{2\pi}{\lambda}(x - t)\right) \end{aligned}\right\} \tag{25a}$$

$$\left.\begin{aligned} L_1 = -\frac{f}{2}, L_2 + \alpha L_3 = -1, L_5 = 1, L_7 = 1, L_9 = 1 \\ at\ y = h_2 = -d - b\,Cos\left(\frac{2\pi}{\lambda}(x - t) + \varphi\right) \end{aligned}\right\} \tag{25b}$$

A MATLAB solved named bvp5c is utilized for the numerical computation. The convergence is set to the 5th power of 0.1 and the step size of the iteration is assumed to be 0.001. This ensures that the convergence of solution and accuracy is maintained. The detail methodology adapted is depicted in flow diagram as shown in Fig. 2.

The findings of the research carried out in Refs. [21,22] are in good agreement with the magnetic factor values that were obtained as shown in Table 1.

4. Physical phenomena of factors on flow profiles

The peristaltic flow of nanoliquid within sinusoidal channel for the existence of porous substance is analyzed in the current study. Particularly, the Phan-Thein-Tanner (PTT) non-Newtonian model with the implication of Hall current and the coupling effect of Soret and Dufour is presented in this article. Moreover, the radiating energy influence with the mixed convection effect enriches the flow properties of the non-Newtonian fluid. The particle concentrations of the gold nanoparticles have greater impact on the fluid velocity and temperature distribution. The modified model incorporating defining parameters is handled numerically and in particular "Shooting-based Runge-Kutta fourth-order" is adopted for the solution employing bvp4c in MATLAB environment. Further, the physical behvaior of the contributing factors is depicted via graphs and elaborated briefly.

The noteworthy physical significance of diversified issues on the flow process are visualized in different figures. Fig. 3 describes the characteristic of magnetization (M) affecting the momentum distribution of the non-Newtonian fluid. The factor M is distributed within certain range and it is described as $0 \leq M \leq 3$. Particularly, $M = 0$ is utilized for the non-occurrence of the magnetic field affecting the momentum of the fluid and the profile is showcased for the existence of other body forces. Further, $M \neq 0,$ signifies the consequence of magnetic factor affecting the fluid momentum within the channel. The behavior of the momentum distribution varies differently in different domain and the profile is divided into three distinct regions. In particular near to the lower wall and upper wall along with the middle region the profile intersects and it is clear to see that near the walls of the channel the profile increases showing a significant retardation in the channel width. Further, in the central region also the profile attenuates with the increasing magnetization. The fact is because of the increasing $M,$ the occurrence of resistivity due to the Lorentz force the profile retards and the axial velocity distribution retards significantly. A larger pressure gradient is required for the enhanced magnetization occurring the flow resistance to maintain the same flow rate. This phenomenon is crucial for the flow of blood in arteries when exposed to magnetic field i. e. in magnetic drug targeting and hyperthermia treatment. The Hall effect in peristaltic transport is applicable in microfluidic devices.

Figs. 4–6 respectively presents the role of thermal $(Gr_t),$ solutal Grashof number $(Gr_c),$ and Soret Grashof number (Gr_f) on the fluid velocity which is useful in peristaltic transport of blood. In both of the figures the variation of the factors are presented as $0 \leq Gr_t, Gr_c, Gr_f \leq 3$. Particularly, $Gr_t = Gr_c = Gr_f = 0$ presents the absence of buoyant forces on the flow phenomena and the graphical illustration reveals that the profile thickness near to the lower wall is thinner whereas near the upper wall its trend is reverse. Moreover, the non-zero variation demonstrates the key attributes of the velocity distribution. Both the buoyant forces and their occurrence are because of the density variations within the fluid layers and this density causes a pressure differential between the layers. The pressure at the bottom is dominated by the pressure at the upper layer of the fluid within the channel and therefore, the increasing buoyancy overshoots the profile and it moves from the lower towards the central region. This indicates the greater increase in the velocity near the lower wall which leads to increasing thickness. However, from the central region with a point of inflection the profile shows its opposite impact. In the human body, both the buoyant forces significantly impact gastrointestinal fluid motion and mucus transport in airways. Further, thermal buoyancy is useful in enhanced oil recovery where peristaltic pumping is used to transport crude oil. The

Table 1
Comparison of heat transportation coefficient for different values of M

M	Results of [21]	Results of [22]	Present
2	1.94404	1.944	1.944044
3	2.13528	2.1353	2.135463
4	2.38482	2.3848	2.384468

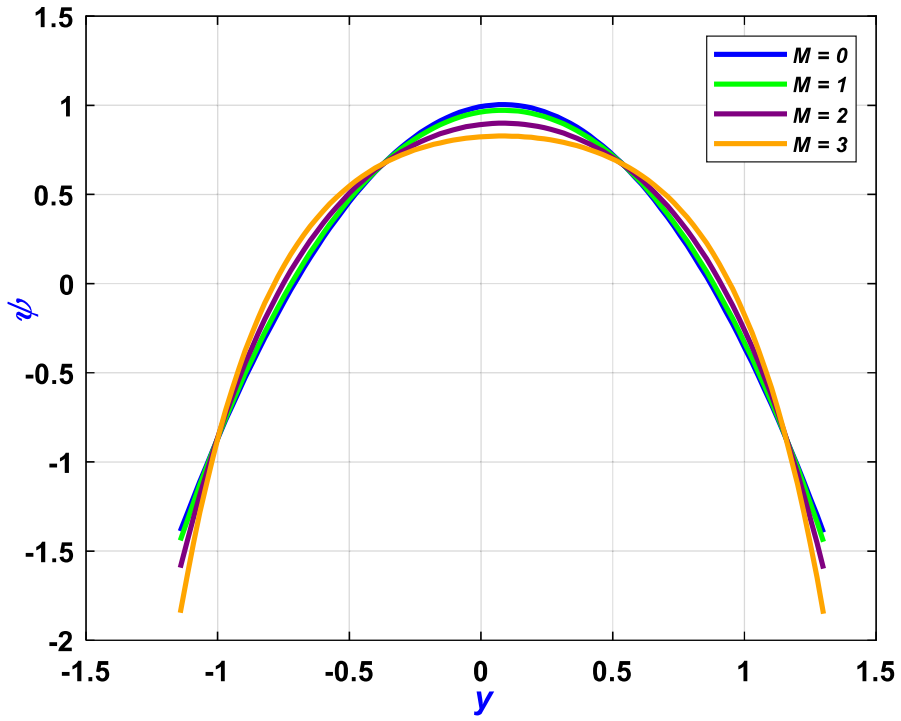

Fig. 3. Deviation of M on u

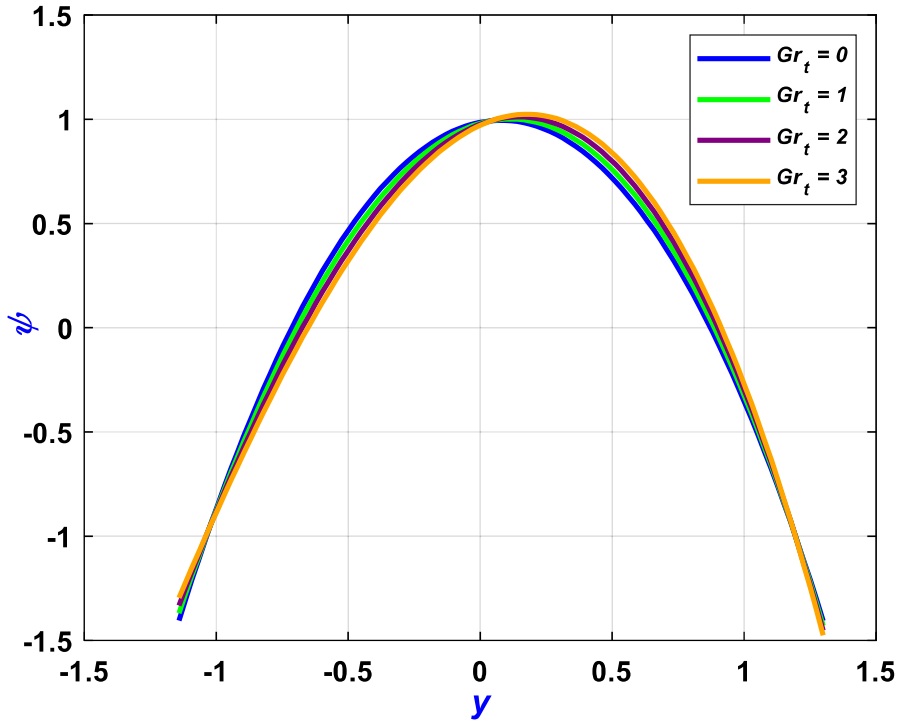

Fig. 4. Deviation of Gr_t on u

non-Newtonian behaviour of the proposed viscoelastic model is deployed for the variation of Weissenberg number on the fluid velocity. Fig. 7 illustrates the assessment of Weissenberg number on the velocity distribution of peristaltic flow. The assigned numerical result of *We*, $We = 0$ shows the behaviour of Newtonian fluid and the non-Newtonian results are depicted for the non-zero assigned values of *We*. The non-Newtonian behaviour due to the increase of We dominates the behaviour of Newtonian fluid and the results are deployed in three distinct regions. It is seen that closed to the wall region the profile enhances greatly with decreasing the wall thickness whereas the profile of central region also attenuates smoothly for the increasing Weissenberg number. The pattern seems to